Published in final edited form as:
J Am Chem Soc. 2009 June 10; 131(22): 7678–7684. doi:10.1021/ja809777j.

A Comparative PCET Study of a Donor-Acceptor Pair Linked by Ionized and Non-ionized Asymmetric Hydrogen-Bonded Interfaces

Elizabeth R. Young, **Joel Rosenthal**, **Justin M. Hodgkiss**, and **Daniel G. Nocera**
Department of Chemistry, 6-335, Massachusetts Institute of Technology, 77 Massachusetts Avenue, Cambridge, MA 02139-4307

Daniel G. Nocera: nocera@mit.edu

Abstract

A Zn(II) porphyrin-amidinium is the excited state electron donor (D) to a naphthalene diimide acceptor (A) appended with either a carboxylate or sulfonate functionality. The two-point hydrogen bond (---[H^+]---) formed between the amidinium and carboxylate or sulfonate establishes a proton-coupled electron transfer (PCET) pathway for charge transfer. The two D---[H^+]---A assemblies differ only by the proton configuration within the hydrogen bonding interface. Specifically, the amidinium transfers a proton to the carboxylate to form a non-ionized amidine-carboxylic acid two-point hydrogen network whereas the amidinium maintains both protons when bound to the sulfonate functionality forming an ionized amidinium-sulfonate two-point hydrogen network. These two interface configurations within the dyads thus allow for a direct comparison of PCET kinetics for the same donor and acceptor juxtaposed by an ionized and non-ionized hydrogen-bonded interface. Analysis of PCET kinetics ascertained from transient absorption and transient emission spectroscopy reveal that the ionized interface is more strongly impacted by the local solvent environment, thus establishing that the initial static configuration of the proton interface is a critical determinant to the kinetics of PCET.

Introduction

Proton-coupled electron transfer (PCET) networks can be established by using an amidine and carboxylic acid to juxtapose a donor to an acceptor. Unlike symmetric interfaces[1,2] or those that cannot support proton transfer,[3,4] the asymmetric nature of the amidine-carboxylic acid interface underscores the importance of the proton configuration on PCET[5-9] by adding a dipole component to the proton interface.[10,11] Proton fluctuations within the hydrogen-bonding interface couple to the charge shift accompanying the electron transfer through the polarization of the surrounding environment.[12-22] Even in the absence of proton transfer, fluctuations of the proton position within the interface profoundly influence the kinetics of the electron transfer component of PCET.[9,23] An especially important issue in biology is the effect of ionization on charge transport rates. Electron transfer may be dramatically altered by the direction of the transferring electron with regard to the orientation of electrostatic and polar fields within the biological milieu.[24-27] In addition, amino acid radical transport rates and yields depend on the ionization state of the amino acid.[28-30] To date, the issue of ionization on PCET has not been isolated owing to the inability to perform comparative

Correspondence to: Daniel G. Nocera, nocera@mit.edu.

Supporting Information **Available.** Fitting and kinetic modeling of transient absorption data is provided in the supporting information. Additional variable temperature data for 1, 1:benzoate and 1:phenylsulfonate are summarized and reported in the supporting information section. This information is available free of charge via the Internet at http://pubs.acs.org/.

PCET rate measurements on a homologous system that features ionized vs. non-ionized proton interfaces.

The two-point hydrogen bond between amidine and carboxylic acid gives rise to the possibility of two proton interface configurations: a non-ionized amidine-carboxylic acid interface or an ionized amidinium-carboxylate interface, both of which are shown in Scheme 1. The proton configuration within the interface has been determined by using a highly conjugated amidinium-appended porphyrin, which exhibits distinctive shifts in the absorption spectrum depending on the protonation state of the amidine functionality.[31] Systematic study of a series of binding moieties has shown that the equilibrium configuration of the proton within the interface is dependent on a balance between the pK_a of the bound acid and the electrostatic energy engendered by the dipole interface.[32] For the case of a sulfonic acid, the pK_a difference is sufficiently large that the ionized amidinium-sulfonate tautomer is preferred in organic solvent of relatively low dielectric constant. Conversely, carboxylic acids yield the neutral amidine-carboxylic acid configuration under the same conditions. With the different tautomeric configurations established, the effect of the proton interface configuration on PCET can be examined. We now report the comparative PCET kinetics for a Zn(II) porphyrin photo-donor (**1**) appended with an amidinium juxtaposed to a naphthalene diimide acceptor functionalized with a carboxylate (**3**) or sulfonate (**4**) functionality; the corresponding dyads are depicted in Scheme 2. The work reported herein augments previous PCET and isotope kinetics measurements of **1:3**.[8,9] In undertaking kinetics rate measurements for **1:4**, the effects of interface architecture and configuration on the PCET dynamics may be considered and analyzed. We show that the local solvent environment has a large impact on the PCET kinetics of assemblies of identical donor-acceptor pairs but with different proton configurations within the interface.

Experimental Section

Materials

Silica gel 60 (70 - 230 and 230 - 400 mesh, Merck) and Merck 60 F254 silica gel (pre-coated sheets, 0.2 mm thick) were used for column and analytical thin-layer chromatography, respectively. Solvents for synthesis were of reagent grade or better and were dried according to standard methods.[33] Spectroscopic experiments employed tetrahydrofuran (THF) (Spectroscopic grade), which was dried using standard methods and stored under vacuum. Deuteration of the interface to form **1-D** from **1-H** (protonated amidinium interface) was accomplished by addition of D_2O from individual ampoules (Cambridge Isotope Laboratories). Preparation of **1-H**[34] and naphthalene diimide-carboxylate **3**[8] have been reported previously. Mass spectral analyses were performed in the MIT Department of Chemistry Instrumentation Facility (DCIF) or at the University of Illinois Mass Spectrometry Laboratory.

Physical measurements

^{1}H NMR spectra were recorded at 25 °C in the MIT DCIF on a Varian XL-500, Unity 300 or Mercury 300 spectrometer. All chemical shifts are reported using the standard δ notation in parts-per-million; positive chemical shifts are to higher frequency from the given reference. Absorption spectra were obtained using a Spectral Instruments 440 Series spectrophotometer. Steady-state emission spectra were recorded on an automated Photon Technology International (PTI) QM 4 fluorimeter equipped with a 150 W Xe arc lamp and a Hamamatsu R928 photomultiplier tube.

Electrochemical experiments were carried out using a Bioanalytical Systems (BAS) Model CV-50W potentiostat/galvanostat. Cyclic voltammetry and differential pulse voltammetry were performed in a two-compartment cell using a glassy carbon disk as the working

electrode, a Ag/AgCl reference electrode and a platinum wire auxiliary electrode. The supporting electrolyte used for electrochemistry experiments was either 0.1 M *n*-tetrabutylammonium hexafluorophosphate ($TBAPF_6$) or perchlorate (TBAP). The solution in the working compartment of the cell was deaerated using nitrogen. Background cyclic voltammograms of the electrolyte solution were recorded prior to addition of the solid sample. Redox couples were referenced to SCE by using a ferrocenium/ferrocene internal standard of 0.307 V vs SCE.[35]

The excitation source for transient absorption (TA) and luminescence lifetime measurements was a chirped-pulse amplified Ti:Sapphire laser system that has been described elsewhere.[8] In this experiment, the 100-fs, 800-nm output of the regenerative amplifier was frequency-upconverted in a visible optical parametric amplifier (BMI Alpha-1000) to produce a 1 kHz pulse train of excitation pulses at 560 nm for resonant excitation of the Q-band of **1**. The excitation was vertically polarized and attenuated to 50 - 250 nJ/pulse.

Transient absorption spectroscopy was performed on samples contained in a high-vacuum cell comprising a 1-cm pathlength clear fused-quartz cuvette (Starna cells) connected to a 10-cm^3 solvent reservoir via a graded seal. High-vacuum Teflon valves were used to seal the cell from the environment and the cuvette from the solvent reservoir. The TA spectrum of **1-H:3** has been previously reported.[8] Single wavelength TA spectroscopy for **1-H:4** is reported here. One aliquot of **1** (1×10^{-7} moles) was added to the cuvette and a two-equivalent aliquot of **4** (2×10^{-7} moles) was added to the solvent reservoir. The cell was evacuated under high-vacuum (10^{-5} torr) to remove the transferring solvent and to leave the two compounds in their separated compartments. One-half milliliter of dry THF was added to the solvent reservoir by high vacuum transfer and the solvent was subject to three cycles of freeze-pump-thaw. The cell was sealed from the environment and removed from the high vacuum manifold. Single wavelength TA experiments were first performed on unbound **1-H** under vacuum using resonant excitation of the Q-band of **1** at 560 nm. The isosbestic point ($\lambda_{isobestic}$ = 654 nm) for singlet-triplet conversion yield was determined. At this wavelength, the intensity of the TA spectrum was invariant and thus provided the best wavelength for detecting PCET transients.[8] Subsequently, the Teflon stopper between the cuvette and solvent reservoir was opened and the two compounds were mixed while maintaining vacuum inside the cell to allow for study of the **1-H:4** dyad.

Single wavelength TA experiments were performed with the pump beam mechanically chopped at 500 Hz. The probe beam was spectrally resolved in a Jobin-Yvon Triax 320 monochromator, which was used to select a single wavelength (2 nm) for measurement on an amplified photodiode. The probe beam served as an input signal for a digital lock-in amplifier (Stanford Research Systems SR830) locked to 500 Hz. Data was collected at 10 ps and 50 ps steps over a range of 3 ns and included some negative time points. The results of twenty forward and backwards scans along the stage were collected and averaged.

Samples for variable temperature experiments were prepared following a detailed procedure outlined previously.[9] To summarize, one aliquot (1×10^{-7} moles) of **1-H** was dissolved in a minimal amount of THF and transferred to a borosilicate short-stem glass ampoule (Kimble-Kontes). Prior to the transfer, a few drops of D_2O were added to samples for deuterium isotopic exchange experiments. The samples were sealed from the atmosphere, shaken and left for 15 minutes before being transferred to the ampoule. The neck of the ampoule had been stretched with a flame to reduce the diameter and allow for easier sealing after high vacuum manipulations. Addition of 4 equivalents of benzoate, 4 equivalents of **3**, 8 equivalents of phenylsulfonate or 8 equivalents of **4** were added for control and quenching experiments. The ampoule containing the sample was attached to a high vacuum adaptor. The transferring solvents were removed on a high vacuum manifold ($< 10^{-6}$ Torr) and the

sample remained under vacuum for at least 2 hours to remove any residual water. One milliliter of dry THF was added to the ampoule by vacuum transfer and was subject to at least three cycles of freeze-pump-thaw. The ampoule was then flame-sealed while the solvent remained frozen. The high-vacuum manipulations were necessary to ensured that the samples remained free from exposure the environment or water, which disrupts the hydrogen bonding between the dyads.

Variable temperature measurements were carried out as described previously.[9] A modular cryogenic refrigeration system (Air Products and Chemicals) consisting of a single stage helium compressor (model 1RO2A) connected via hoses to an expander module (model DE-202) with a heating element and temperature controller (Scientific Instruments, 9600-5) was interfaced with a custom-made computer program in order to automate the temperature control settings. The expander module is housed within in laboratory interface (model DMX-1) consisting of a vacuum shroud with glass windows for fluorescence spectroscopy in a right-angle configuration and is continuously pumped to maintain a vacuum ($\sim 10^{-4}$ torr). The ampoule containing the sample is mounted on a copper block and the thermocouple was calibrated at three temperatures: liquid nitrogen (77 K), an ice bath (273 K) and ambient temperature (293 K).

Luminescence lifetime kinetics were measured on a Hamamatsu C4334 Streak Scope streak camera that has been described elsewhere.[36] The emission was collected at the magic angle ($\theta_m = 54.7^\circ$) over a 140-nm window centered on the emission peak. A 10-ns or a 20-ns time base was used.

Data acquisition was automated for the variable temperature experiments. The temperature controller and streak camera were synchronized to enable data collection throughout the entire temperature range. Luminescence measurements were made after a 20 minute wait time during which the temperature was adjusted and the sample was allowed to equilibrate. This cycle occurred for each temperature data point, which was typically 10-25 K apart. Each sample was cycled through the entire temperature range 4 times in different sequences to ensure that the data was independent of the sequence.

Temperature-dependent lifetimes of **1-H(D)** alone and bound to benzoate or phenylsulfonate were measured over a temperature range of 120-300 K. Experiments were repeated at least 3 times with newly prepared samples. Luminescence lifetimes were determined from streak camera data analysis by integrating 15-nm or 13-nm, or 40-nm or 50-nm slices of the emission peaks centered at 612 and 655 nm, for **1:3** and **1:4** respectively, and fitting to a monoexponential decay function. Temperature dependent lifetimes of **1-H(D):3** and **1-H(D):4** were measured at the same temperature points and the data was fit in the same manner, except that the data was fit to a biexponential decay function with the longer lifetime component fixed to the lifetime obtained from the control experiment, **1-H(D)**, at each temperature.

Synthesis of naphthalene monoanhydride (2)

1,4,5,8-Naphthalenetetracarboxylic acid dianhydride (8.95 g, 33.4 mmol) and 2,5-di-*tert*-butylaniline (3.2 g, 15.6 mmol) were combined in a 250 mL round-bottom flask. To the mixture of reactants was added 75 mL of anhydrous DMF. The resulting solution was stirred under an atmosphere of nitrogen and heated at 105 °C, for 14 h. After the dark solution was cooled to room temperature, the DMF was removed under reduced pressure. The resulting residue was purified by column chromatography on silica using a solution of 10% ethyl acetate in hexanes as the eluent to remove nonpolar impurities. The desired product was isolated using ethyl acetate and hexanes (1:1) as the eluent to generate 1.34 g of the title

compound in 19% yield. ^{1}H NMR (300 MHz, $CDCl_3$) δ/ppm: 8.84 (s, 4H), 7.62 (dd, *J* = 8.5 Hz, 1H), 7.53 (dd, *J* = 8.5, 2.2 Hz, 1H), 7.01 (d, *J* = 2.2 Hz, 1H), 1.33 (s, 9H), 1.25 (s, 9H).

Synthesis of naphthalenediimide (4)

A solution of monoanhydride **2** (2.0 g, 4.40 mmol), and aminomethanesulfonic acid (3.1 g, 28.0 mmol) in DMF (40 mL) was refluxed under a nitrogen atmosphere for 16 h. The solution was then cooled to room temperature and concentrated under reduced pressure. The crude material was redissolved in CH_2Cl_2 and washed with 5% HCl. The organic layer was then separated, and the aqueous layer was extracted twice with 50 mL of CH_2Cl_2. The organic layers were combined, dried over Na_2SO_4 and reconcentrated under reduced pressure. The resultant residue was chromatographed on silica gel with CH_2Cl_2 to remove nonpolar impurities and then with CH_2Cl_2 and MeOH (75:1 v:v) to furnish the desired product, which was recrystallized from CH_2Cl_2 and hexanes. The purified product was filtered and washed with cold CH_2Cl_2 and hexanes (1:3 v:v) to afford the pure sulfonic acid diimide in 17% yield (0.41 g). ^{1}H NMR (300 MHz, CD_3OD, 25 °C) δ/ppm: 8.79 (dd, J_1 = 7.5, J_2 = 7.1, 4H), 7.58 (d, J = 5.3 Hz, 1H), 7.48 (dd, J_1 = 3.7 Hz; J_2 = 1.5 Hz, 1H), 7.18 (d, J = 1.1 Hz, 1H), 5.42 (s, 2H), 1.31 (s, 9H), 1.23 (s, 9H). ESIMS $[M - H^+]^-$ calcd for $C_{29}H_{27}N_2O_7S$ *m/z*: 547.1539, found 547.1517.

The sulfonic acid appended diimide was converted to the corresponding sulfonate salt by dissolving 123 mg (0.240 mmol) of the acceptor in 25 mL of 2% MeOH in CH_2Cl_2 and cooling the resultant solution to −78 °C. In dropwise fashion, 100 μL of tetramethylammonium hydroxide (TMAOH) (25% in MeOH) was added to the cold stirring solution, which was stirred for an additional 5 minutes at −78 °C and then warmed to room temperature. Concentration of the solution under reduced pressure yielded a solid, which was dried for 14 h under vacuum. A pure product was obtained in quantitative yield. ^{1}H NMR (300 MHz, CD_3OD, 25 °C) δ/ppm: 8.79 (dd, J_1 = 7.5, J_2 = 7.1, 4H), 7.58 (d, J = 5.3 Hz, 1H), 7.48 (dd, J_1 = 3.7 Hz; J_2 = 1.5 Hz, 1H), 7.18 (d, J = 1.1 Hz, 1H), 5.42 (s, 2H), 3.04 (s, 12H),1.31 (s, 9H), 1.23 (s, 9H). ESIMS $[M - N(CH_3)_4^+]^-$ calcd for $C_{29}H_{27}N_2O_7S$ *m/z*: 547.1539, found 547.1553.

Results

The supramolecular dyads designed for comparative PCET kinetics investigations, displayed in Scheme 2, are formed from the association of a Zn(II) porphyrin-amidinium donor to naphthalene diimide acceptors **3** and **4**. These acceptors are prepared according to the reaction sequence depicted in Scheme 3. 2,5-di-*t*-Butylaniline is condensed with 1,8:4,5-napthalenedianhydride in refluxing DMF to generate the asymmetric monoanhydride **2**,[37] which can subsequently be condensed with either glycine or aminomethanesulfonic acid to generate **3** or **4**, respectively. Supramolecular dyads of these diimide acceptors form a well-defined two-point hydrogen bond that possesses favorable primary and secondary electrostatic interactions.[38] A signature of this hydrogen bonding association is the downfield shift of amidinium protons involved in hydrogen bonding (NH_{ax}) and an insensitivity of the chemical shift of the amidinium protons external to the salt bridge (NH_{eq}). As previously demonstrated for the ^{1}H NMR spectrum for the Ni(II) derivative of the **1:3** complex in 2Me-THF,[8] the NH_{ax} protons move downfield from 10.6 to 12.4 ppm upon their hydrogen bonding association to the carboxylate, whereas the chemical shift of the NH_{eq} protons changes by <0.05 ppm. A similar downfield shift in the ^{1}H NMR spectrum of **1** induced by the addition of **4** (from 10.6 to 12.1 ppm) in THF confirms that binding in the **1:4** dyad occurs through the two-point hydrogen bond (as opposed to axial ligation) of the amidine-sulfonic acid interface. THF binds axially to Zn(II) porphyrins thereby preventing porphyrin aggregation caused by axial ligation of the amidine to the Zn(II)

porphyrin. Accordingly, the solvent enforces a two-point hydrogen bond as the only structure for dyad assembly.

The association of **1** to **3** in 2Me-THF has been previously been determined to be K_{assoc}(**1-H:3**) = 2.8×10^4 M^{-1} from the analysis of the ratio of pre-exponential factors of the transient emission (TE) decay curves of **1** with varying concentrations of **3**.[9] Because measurements reported herein are in THF, we determined K_{assoc}(**1-H:3**) in THF. The static fluorescence quenching from the porphyrin chromophore was monitored upon titration of **1** with **3**. A fit of the emission intensity to the Benesi-Hildebrand equation yields K_{assoc}(**1-H:3**) = 2.4×10^4 M^{-1} (THF, 298 K),[8] which closely matches that derived from the ratio of pre-exponential factors of the bound:unbound lifetimes of **1**.[39] As expected, K_{assoc}(**1-H:3**) in 2Me-THF and THF are similar. With the validity of the lifetime method established, the binding of **1-H** to **4** was determined by analysis of the pre-exponential factors of the emission lifetime decay curves to give K_{assoc}(**1-H:4**) = 2.9×10^2 M^{-1} in THF. The ratio of pre-exponential factors remains similar from 150 to 300 K indicating that **4** remains bound to **1** throughout the sampled temperature range.

Figure 1 shows the TA kinetics profiles measured at λ = 654 nm for **1** and dyad **1-H:4** in THF. Following excitation of the $Q_{1,0}$ band of **1**, a broad TA feature of the porphyrin S_1 excited state is superimposed on bleaching features at 562 and 602 nm that arise from the loss of the ground-state Q-band absorptions. Single wavelength TA kinetics in this region show decay profiles arising from intersystem crossing to the T_1 excited state, which can obscure the spectral signatures of PCET intermediate (porphyrin radical cation, λ_{max} = 412 and 637 nm;[8] and diimide radical anion, λ_{max} = 475 and 610 nm[40]). An isosbestic point in the S_1-T_1 TA spectra of unbound **1** provides a dynamic-free background for single-wavelength observation of the porphyrin radical cation, as previously demonstrated in PCET studies of **1:3**.[8] Accordingly, TA was employed in an effort to observe the growth and decay of an optical signature attributed to the porphyrin radical cation of the charge-separated state for the **1:4** dyad at λ_{obs} = 654 nm, the isosbestic point for S_1-T_1 conversion. The dynamics of charge separation in Figure 1 are superimposed on the flat S_1-T_1 absorption profile arising from unbound **1** in solution. Based on K_{assoc}(**1:4**) in THF (3.5×10^2 M^{-1}), ~25% of the porphyrin is bound by the acceptor at the concentrations used for TA experiments. The single wavelength TA kinetics trace for **1:4** shows a shoulder with shallow decay instead of a clear growth and subsequent decay as obtained for **1:3**. Nevertheless, the TA profile does contain components of 1) formation of the porphyrin radical cation in forward ET followed by 2) depletion of the radical cation via back electron transfer. A bi-exponential fit to the data was performed by fixing one lifetime component to the forward ET lifetime (τ_{em} = 420 ps), which was obtained by time resolved fluorescence quenching experiments. This treatment of the data yields k_{ET}(forward) = 2.4×10^9 s^{-1} (298 K) for the growth of the transient signal and k_{ET}(back) = 3.3×10^9 s^{-1} (298 K) for the transient signal's disappearance. Details of the kinetics analysis are provided in the SI section. The rate constants for **1:4** are significantly greater than the corresponding rates recorded for **1:3** of k_{ET}(forward) = 0.9×10^9 s^{-1} (2Me-THF, 298 K) and k_{ET}(back) = 1.4×10^9 s^{-1} (2Me-THF, 298 K), respectively. For **1:4**, accumulation of the charge-separated intermediate is not significant owing to the faster overall kinetics of the **1:4** system as well as k_{ET}(back) > k_{ET}(forward). Kinetic modeling of TA signatures upon variation of k_{ET}(forward) and k_{ET}(back) was performed and is presented in the SI. At the experimental concentrations employed, for the case in which k_{ET}(back) > k_{ET}(forward), the growth of a charge-transfer intermediate TA signal appears as a shallow rise with subsequent decay (such a feature is observed in Figure 1) instead of a distinct rise and decay as reported previously **1:3**. As discussed in the SI, the shallow rise is a general characteristic of faster ET kinetics and k_{ET}(back) > k_{ET}(forward).

Temperature-dependent rate constants were ascertained from transient emission (TE) decay kinetics. The fluorescence lifetimes of **1-H** (protonated amidinium) and **1-D** (deuterated amidinium) in THF increase linearly with decreasing temperature (Figure S5). Phenylsulfonate (**PS**) binds efficiently to **1**, but it is not capable of quenching the S_1 excited state of **1** via electron or energy transfer. The **1-H**(**D**):**PS** dyad thus allows the dynamics of **1** to be ascertained in the presence of a two-point hydrogen bond but in the absence of excited state deactivation due to PCET dynamics. The lifetime of the **1-H**(**D**):**benzoate** and **1-H**(**D**):**PS** dyads (Figure S6) correspond well with the temperature dependence of **1** alone, and all lifetime versus temperature plots show similar slopes, indicating that formation of the two-point hydrogen bond does not affect the excited state dynamics of the Zn(II) porphyrin amidinium. Conversely, the TE decay profile is dramatically perturbed when the benzoate or **PS** binding moieties are replaced by **3** and **4**, respectively. Fluorescence decays of **1-H**(**D**):**3** and **1-H**(**D**):**4** exhibit a biexponential decay functional with one time constant fixed to the unquenched lifetime of **1-H**(**D**) and the second lifetime varied to obtain the best fit. The lifetime of unbound **1** was independently determined at all temperatures at which PCET measurements were made. The quenched time constant was used to determine the forward rate of PCET using the relation $k_{PCET} = (1/\tau_{1\text{-}\mathbf{H(D)}:\mathbf{Q}}) - (1/\tau_{1\text{-}\mathbf{H(D)}})$, where **Q** = **3** or **4**. Figure 2 plots k_{PCET} values versus temperature for protonated PCET dyads **1:3** and **1:4** in THF. Deuterated data plotted in manner has been omitted for clarity as it appears in Figure 3. Figure 3 presents the protonated and deuterated data in an Arrhenius plot of the form $\ln(k_{PCET} \cdot T^{1/2})$ versus 1/T fitted with the semi-classical Marcus formalism. Linear Arrhenius behavior is observed. A distinct isotope effect is seen for each sample indicating that the photoinduced charge transfer is sensitive to nuclear motions within the intervening proton interface. In the previously reported study of **1-H**(**D**):**3** in 2Me-THF, the KIE exhibits disparate behavior with variations in temperature.[9] In the high-temperature regime (300 K), KIE (k_H/k_D) ~ 1.22(1) whereas in the low-temperature regime (120 K), the isotope dependence inverts to KIE ~ 0.87(1). As shown in Figure 3, KIE for **1-H**(**D**):**3** and **1-H**(**D**):**4** in THF also exhibits non-parallel behavior over the temperature range studied.

Discussion

The influence that intervening hydrogen bonds exert on charge transfer kinetics is revealed when **1:3** (Scheme 2) is compared to a closely related system in which the donor and acceptor sites are covalently bound. Introduction of hydrogen bonds between D—A moieties retards ET rates by over two orders of magnitude. This effect is primarily ascribed to the attenuation of the electronic coupling constant, $|V|$. The previously reported value of $|V| \sim 2$ cm^{-1} determined for **1:3** is 10-fold smaller than that inferred for covalently bound analogues.[9,41-44] This observation is reaffirmed by $|V|$ values from ~ 4 cm^{-1} to 12 cm^{-1} for other hydrogen bonded D---[H^+]---A architectures involving three point hydrogen bonded Watson-Crick base pairs.[41-46] Whereas it is clear that hydrogen bonds in D---[H^+]---A systems attenuate charge transfer kinetics and D—A coupling, it is not apparent how the internal structure of the two-point hydrogen bonded interface perturbs the parameters that control PCET. To determine these effects, solvent and temperature dependent studies on the **1:3** and **1:4** dyads were undertaken.

Comparison of PCET kinetics for **1:3** and **1:4** enable an analysis of charge transfer as mediated by differing proton configurations within a hydrogen bonded interface. Previous work involving an amidinium-appended purpurin chromophore allows the assignment of the proton interface configuration in dyads of **1:3** and **1:4**. The amidinium-appended purpurin has been titrated with a series of carboxylate and sulfonate binding moieties to determine the protonation state of the bound amidinium within the assembled interfaces. The pH-dependent UV-vis absorption spectrum of the amindinium-purpurin reveals the manner in which a balance between the pK_a values of the constituent acids and electrostatic

interactions conspire to produce either an ionized or non-ionized interface in THF.[31,32] The results show that **1:3** dyads are bridged by a *non-ionized amidine-carboxylic acid interface* while **1:4** dyads are concatenated by an *ionized amidinium-sulfonate interface*.

Temperature-dependent kinetic data can be analyzed using the semi-classical Marcus equation,[47]

$$k_{ET}=\frac{2\pi}{\hbar}|V|^2\sqrt{\frac{1}{4\pi\lambda k_B T}}\exp\left[\frac{(\Delta G^o+\lambda)^2}{4\lambda k_B T}\right] \quad (1)$$

The activation energy (E_a) of the PCET reaction is furnished by the slope of the kinetics results plotted in the Arrhenius form. The calculated E_a values summarized in Table 1 are small relative to the PCET driving force (ΔG^o), which is known for all systems (Table 1). The total reorganization energies, λ, are determined from the slope of the linear Arrhenius fit as described previously.[9] The values for the reorganization energy range from λ = 0.80 - 0.93 eV for **1-H(D):3** (THF) and **1-H(D):4** (THF). The λ values match well with a calculated reorganization energy comprising an outer-sphere reorganization energy of λ_o ~ 0.8 eV (r_{DA} distance of 13 Å, and ionic radii of 5 and 4 Å for the donor (**1**) and naphthalene diimide acceptors **3** and **4**, respectively) and inner-sphere solvent reorganization contributions of λ_i ~ 0.2 - 0.3 eV for Zn(II) porphyrin donor-diimide acceptor systems.[48,49] With ΔG^o and λ determined, the electronic coupling matrix element, |*V*| was evaluated from the *y*-intercept of the linear fit as per Eq. 1 as has been reported previously.[9] The values of |*V*| listed in Table 1 (|*V*| ~1.9 - 4.5 cm^{-1}) are smaller than the corresponding values determined for covalently bound systems of similar architectural cular topology (|*V*| ~ 10's cm^{-1}).[48,49]

Comparison of the PCET dynamics and parameters for **1:3** and **1:4** underscores the sensitivity of charge transfer through hydrogen bonds to the surrounding environment and highlights the effects that are imposed by structural changes within the proton interface. Both **1:3** and **1:4** maintain a specific asymmetric two-point hydrogen bonded interface joined via N---H---O hydrogen bonding that mediates charge transfer between a Zn(II) porphyrin and naphthalene diimide. The driving force for ET varies by only 0.03 eV among the **1-(H/D):3** and **1-(H/D):4** dyads, which precludes the attribution of the observed changes in PCET behavior to a simple driving force effect. The nature of the static configuration (non-ionized or ionized) of the protonic interface in **1:3** and **1:4** and difference in the coupling through the sp^2-hybridized carbon atom (of carboxylate) versus the sp^3-hybridized sulfur atom (of sulfonate) emerge as two prominent factors that likely modulate the observed solvent and temperature-dependent behavior of PCET in these systems. The difference in the electronic coupling through the interface is one manifestation of the PCET. In the case of **1:4**, the electronic coupling is through an ionized amidinium-sulfonate interface. Presumably, the Coulombic charge of the ionized interface translates to a shorter distance and stronger coupling for **1:4**. Moreover, the internal charge of the ionized amidinium-sulfonate interface of **1:4** induces a pre-organized solvent structure about the proton interface, leading to stronger coupling of the reactants to the solvent. This greater solvent coupling is reflected in a larger reorganization energy of **1:4** as compared to **1:3**. This larger Franck-Condon term is offset by greater electronic coupling thus leading to an overall enhancement in the PCET rate constant for **1:4**. Thus PCET finds its origins in both components of the charge transfer, the electronic coupling and Franck Condon terms.

Modulation of coupling to the solvent is revealed by the kinetic isotope effect (KIE). Note that the slopes of the data plotted for temperature versus rate in the KIE studies are non-parallel. This temperature-dependent behavior of PCET rates can lead to a crossover in the

KIE.[9,50] This unusual phenomenon has been attributed to the freezing out of hydrogen vibrational modes within the interface as temperature decreases. Fluctuations within the hydrogen bonding bridge dynamically modulate electronic coupling for ET, and consequently the rate of charge-separation becomes sensitive to the nature of proton modes within the bridge. The non-parallel slopes in KIE data of **1:3** and **1:4** in THF lead to a ~7% and ~9% increase in KIE over the temperature range sampled. This KIE trend is in contrast to previously reported KIE data reported for **1:3** in 2-MeTHF, which yields a decrease in KIE of ~18% over a similar temperature range.[9] The KIE trend for **1:3** and **1:4** in THF is typical of predictions made by conventional PCET theory.[22,51] The molecular differences between solvents used in these two studies may be a contributing factor in dictating the temperature-dependent behavior and are the focus of continuing research efforts.

In summary, a direct comparison of PCET is facilitated by the similarity of the **1:3** and **1:4** PCET systems such that differences introduced by the two proton interfaces is accentuated. The importance of the proton interface is revealed by the comparative values of λ_s, E_a, and $|V|$ for **1:3** and **1:4**. Stronger coupling of the PCET reaction is observed for interfaces that are ionized. Efforts to measure this solvent coupling directly by 2-D methods are currently underway.

Supplementary Material

Refer to Web version on PubMed Central for supplementary material.

Acknowledgments

J. R. thanks the Fannie and John Hertz Foundation for a predoctoral fellowship. This work was supported by the National Institutes of Health (GM 47274).

References

1. Turró C, Chang CK, Leroi GE, Cukier RI, Nocera DG. J Am Chem Soc. 1992; 114:4013–4015.
2. de Rege PJF, Williams SA, Therien MJ. Science. 1995; 269:1409–1413. [PubMed: 7660123]
3. Sessler, JL.; Wang, B.; Springs, SL.; Brown, CT. Comprehensive Supramolecular Chemistry. Murakami, Y., editor. Vol. 4. Pergamon Press; Oxford: 1996. p. 311-336.and references therein
4. Chang, CJ.; Brown, JD.; Chang, MCY.; Baker, EA.; Nocera, DG. Electron Transfer in Chemistry. Balzani, V., editor. Vol. 3.2.4. Wiley-VCH; Weinheim, Germany: 2001. p. 409-461.
5. Roberts JA, Kirby JP, Nocera DG. J Am Chem Soc. 1995; 117:8051–8052.
6. Roberts JA, Kirby JP, Wall ST, Nocera DG. Inorg Chim Acta. 1997; 263:395–405.
7. Roberts JA, Kirby JP, Nocera DG. J Am Chem Soc. 1997; 119:9230–9236.
8. Damrauer NH, Hodgkiss JM, Rosenthal J, Nocera DG. J Phys Chem B. 2004; 108:6315–6321. [PubMed: 18950117]
9. Hodgkiss JM, Damrauer NH, Pressé S, Rosenthal J, Nocera DG. J Phys Chem B. 2006; 110:18853–18858. [PubMed: 16986876]
10. Cukier RI, Nocera DG. Annu Rev Phys Chem. 1998; 49:337–369. [PubMed: 9933908]
11. Hodgkiss, JM.; Rosenthal, J.; Nocera, DG. Hydrogen-Transfer Reactions. Hynes, JT.; Klinman, JP.; Limbach, HH.; Schowen, editors. Vol. 2.17. Wiley-VCH; Weinheim, Germany: 2007. p. 503-561.
12. Cukier RI. J Phys Chem. 1996; 100:15428–15443.
13. Cukier RI. J Phys Chem. 1994; 98:2377–2381.
14. Zhau XG, Cukier RI. J Phys Chem. 1995; 99:945–954.
15. Cukier RI. J Phys Chem A. 1999; 103:5989–5995.
16. Cukier RI. Biochim Biophys Acta. 2004; 1655:37–44. [PubMed: 15100014]

17. Hammes-Schiffer, S. Electron Transfer in Chemistry. Balzani, V., editor. Vol. 1.1.5. Wiley-VCH; Weinheim, Germany: 2001. p. 189
18. Hammes-Schiffer S. Acc Chem Res. 2001; 34:273–281. [PubMed: 11308301]
19. Hammes-Schiffer S, Iordanova N. Biochim Biophys Acta. 2004; 1655:29–36. [PubMed: 15100013]
20. Soudackov A, Hammes-Schiffer S. J Chem Phys. 1999; 111:4672–4687.
21. Soudackov A, Hammes-Schiffer S. J Chem Phys. 2000; 113:2385–2396.
22. Decornez H, Hammes-Schiffer S. J Phys Chem A. 2000; 104:9370–9384.
23. Pressé S, Silbey R. J Chem Phys. 2006; 124:164504–164511. [PubMed: 16674143]
24. Galoppini E, Fox MA. J Am Chem Soc. 1996; 118:2299–2300.
25. Suydam IT, Snow CD, Pande VS, Boxer SG. Science. 2006; 313:200–204. [PubMed: 16840693]
26. Steffen MA, Kaiqin L, Boxer SG. Science. 1994; 264:810–816. [PubMed: 17794722]
27. Shin YGK, Newton MD, Isied SS. J Am Chem Soc. 2003; 125:3722–3732. [PubMed: 12656602]
28. Seyedsayamdost MR, Yee CS, Reece SY, Nocera DG, Stubbe J. J Am Chem Soc. 2006; 128:1562–1568. [PubMed: 16448127]
29. Seyedsayamdost MR, Reece SY, Nocera DG, Stubbe. J Am Chem Soc. 2006; 128:1569–1579. [PubMed: 16448128]
30. Sibert R, Josowicz M, Porcelli F, Veglia G, Range K, Barry BA. J Am Chem Soc. 2007; 129:4393–4400. [PubMed: 17362010]
31. Rosenthal J, Hodgkiss JM, Young ER, Nocera DG. J Am Chem Soc. 2006; 128:10474–10483. [PubMed: 16895413]
32. Young ER, Rosenthal J, Nocera DG. Chem Commun. 2008:2322–2324.
33. Armarego, WLF.; Perrin, DD. Purification of Laboratory Chemicals. 4th. Butterworth-Heinmann; Oxford: 1996.
34. Yeh CY, Miller SE, Carpenter SD, Nocera DG. Inorg Chem. 2001; 40:3643–3646. [PubMed: 11421722]
35. Bard, AJ.; Faulkner, LR. Electrochemical Methods Fundamentals and Applications. John Wiley; New York: 1980.
36. Loh ZH, Miller SE, Chang CJ, Carpenter SD, Nocera DG. J Phys Chem A. 2002; 106:11700–11708.
37. Iverson BL, Zych AJ. J Amer Chem Soc. 2000; 122:8898–8909.
38. Pranata J, Wierschke SG, Jorgensen WL. J Am Chem Soc. 1991; 113:2810–2819.
39. $K_{assoc} = Q(Q + 1)/([\mathbf{2}]_0(Q + 1) - [\mathbf{1}]_0 Q)$, where Q is the ratio of the pre-exponential factors of the short (bound) and long (unbound) components, which also corresponds to the ratio [**1:3**]/[**1**].
40. Rogers JE, Kelly LA. J Am Chem Soc. 1999; 121:3854–3861.
41. Osuka A, Yoneshima R, Shiratori H, Okada S, Taniguchi S, Mataga N. Chem Commun. 1998:1567–1568.
42. Harrison RJ, Pearce B, Beddard GS, Cowan JA, Sanders JKM. Chem Phys. 1987; 116:429–448.
43. Davis WB, Ratner MA, Wasielewski MR. J Am Chem Soc. 2001; 123:7877–7886. [PubMed: 11493061]
44. Winters MU, Pettersson K, Martensson J, Albinsson B. Chem Eur J. 2005; 11:562–573. [PubMed: 15578692]
45. Sessler JL, Wang B, Harriman A. J Am Chem Soc. 2003; 115:10418–10419.
46. Sessler JL, Sathiosatham M, Brown CT, Rhodes TA, Wiederrecht G. J Am Chem Soc. 2001; 123:3655–3660. [PubMed: 11457097]
47. Marcus RA, Sutin N. Biochem Biophys Acta. 1985; 811:265–322.
48. Archer MD, Gadzekpo VPY, Bolton JR, Schmidt JA, Weedon AC. J Chem Soc Faraday Trans 2. 1986; 82:2305–2313.
49. Gaines GL III, O'Neil MP, Svec WA, Niemczyk MP, Wasielewski MR. J Am Chem Soc. 1991; 113:719–721.

50. Cape JL, Bowman MK, Kramer DM. J Am Chem Soc. 2005; 127:4208–4215. [PubMed: 15783202]

51. Hammes-Schiffer S, Hatcher E, Ishikita H, Skone JH, Soudackov AV. Coord Chem Rev. 2008; 252:384–394. [PubMed: 21057592]

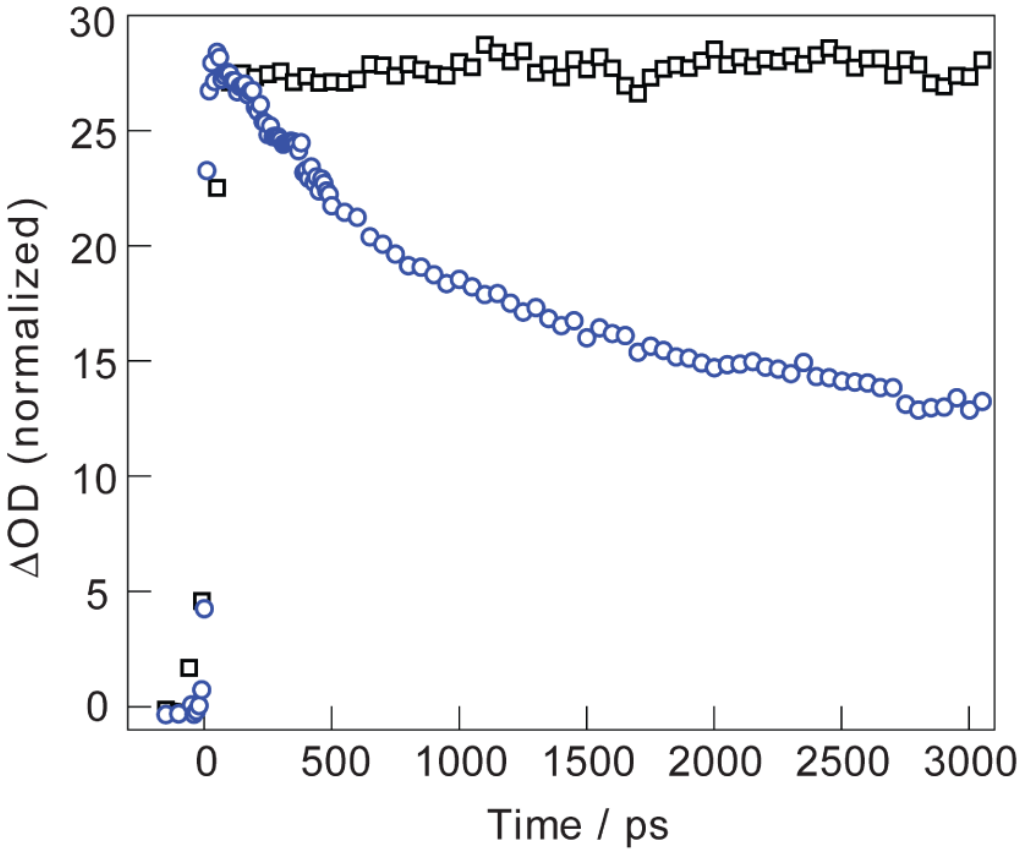

Figure 1.
Single-wavelength transient absorption spectrum of **1** (□) and **1:4** dyad (o) at the $S_1 \rightarrow T_1$ isosbestic point of **1**, λ_{obs} = 654 nm.

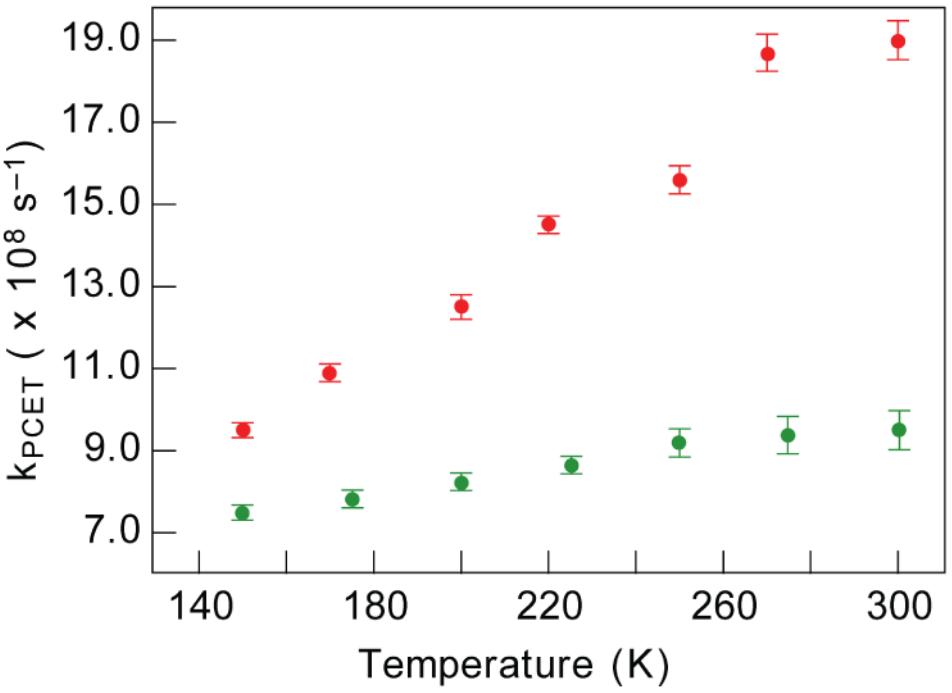

Figure 2.
Temperature dependence of the rate of PCET for **1-H:3** (●) and **1-H:4** (●) dyads in THF.

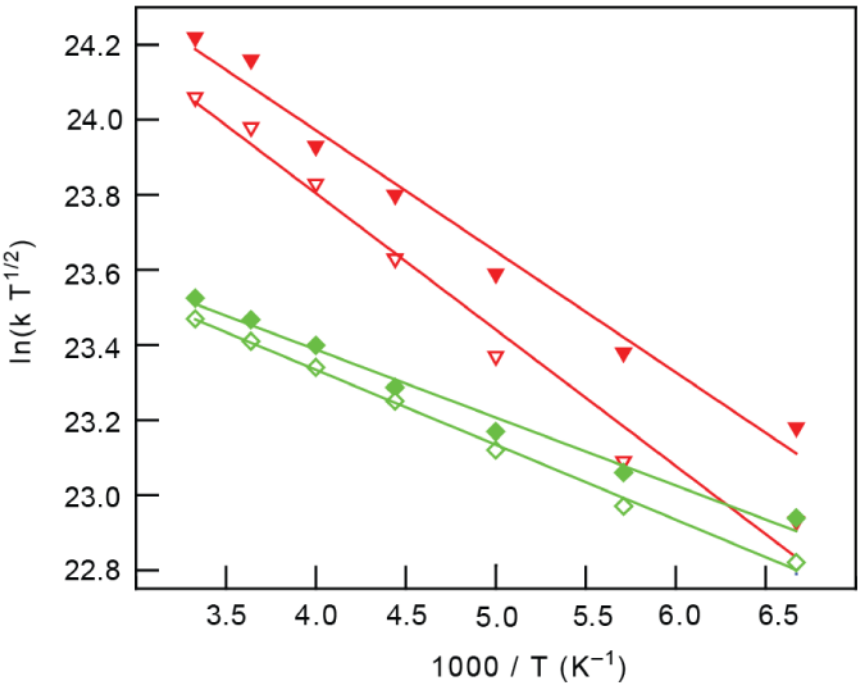

Figure 3.
Arrhenius plot depicting the temperature dependence of the rate of PCET for (a) **1-H:3 (●)** and **1-D:3** (○) in THF and (b) **1-H:4** (●) and **1-D:4** (○) in THF.

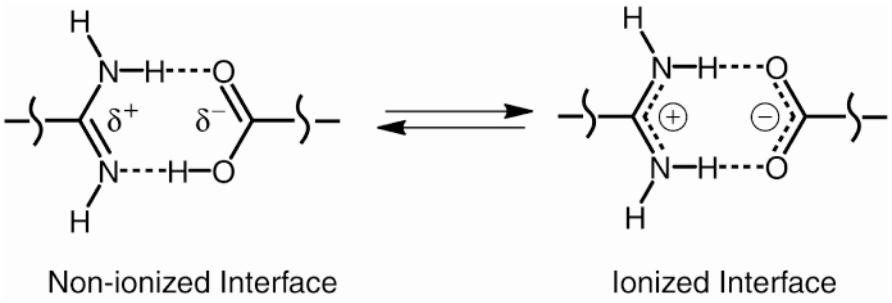

Scheme 1.

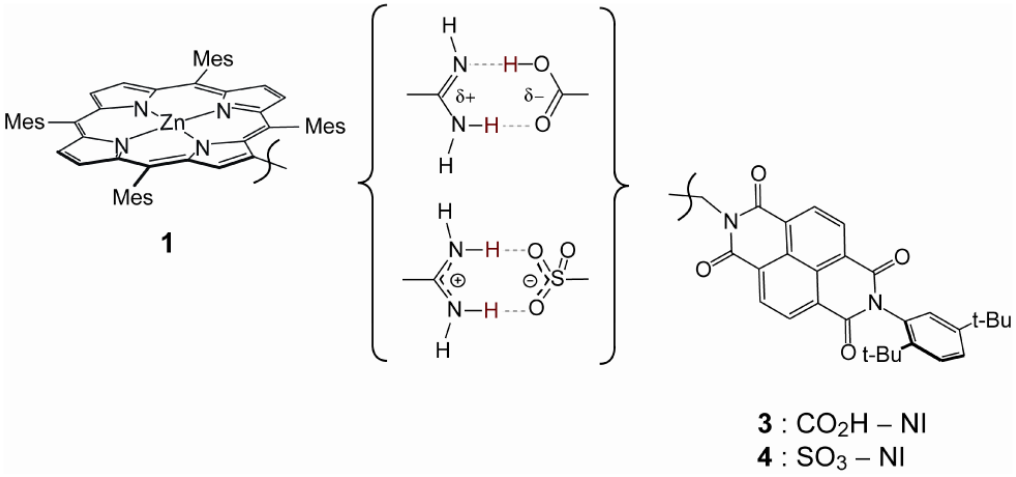

Scheme 2.

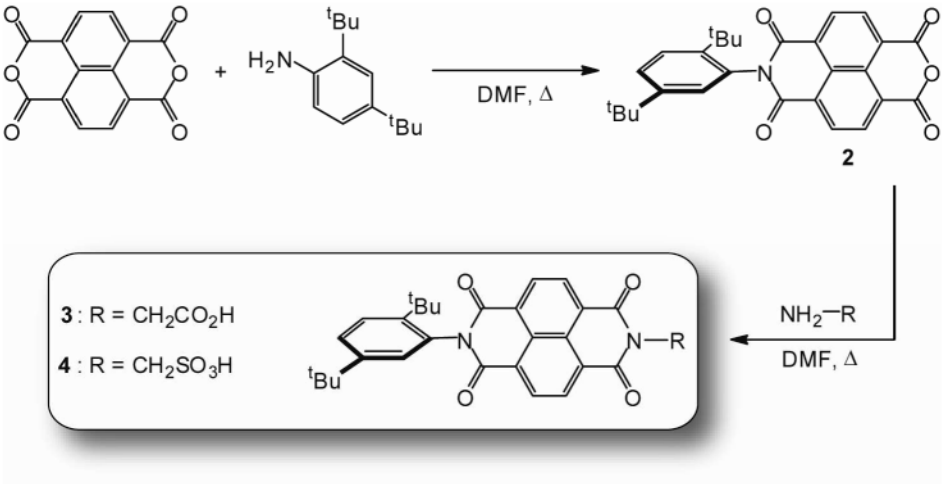

Scheme 3.

Table 1

Thermodynamic and Kinetic Parameters Measured for 1:3 and 1:4 dyads in THF

Dyad	Solvent	ΔG^{o} [a,b] /eV	E_a(obs) [b] /eV	λ_s [b] /eV	$\lvert V \rvert$ [b] / eV [cm^{-1}]	KIE
1-H:3	THF	–0.58	$1.56(9) \times 10^{-2}$	0.80(1)	$3.0(2) \times 10^{-4}$ [2.4(2)]	1.07(1)
1-D:3	THF	–0.58	$1.72(5) \times 10^{-2}$	0.82(1)	$3.1(2) \times 10^{-4}$ [2.5(2)]	
1-H:4	THF	–0.59	$2.8(2) \times 10^{-2}$	0.91(4)	$5.6(9) \times 10^{-4}$ [4.5(8)]	1.22(2)
1-D:4	THF	–0.59	$3.1(2) \times 10^{-2}$	0.93(4)	$5.6(9) \times 10^{-4}$ [4.5(8)]	

[a] Calculation using the expression $\Delta G^{o} = E_D^{ox} - E_A^{red} - E_{ex} + \Delta G(\varepsilon)$ where E_D^{ox} is the oxidation potential of the donor, **1**, E_A^{red} is the reduction potential of the acceptor, **3** or **4**, E_{ex} is the excited state energy of **1** and $\Delta G(\varepsilon)$ is the solvent-dependent Coulombic term. $\Delta G(\varepsilon)$ is calculated from the Born equation for $\varepsilon = 7.52$ (295 K), a D−A distance of 13 Å, and ionic radii of 5 and 4 Å for the donor, **1**, and acceptor, **3** and **4** to yield $\Delta G(\varepsilon) = -0.12$ eV.

[b] Assuming ΔG^{o} is temperature-independent, obtained from fitting results to the semi-classical Marcus equation.

[c] Reported in ref 9.